v_e and v_h are the average thermal velocities of electrons and holes, respectively; and $\eta(-x)$ is the Heaviside step function. Similar analysis for n-type is presented in the supplementary materials.

Figure 3 displays the density distributions in space as a snapshot at t = +20 ps; adding up the distributions for carriers originating in p-type (Fig. 3, B and C) and n-type (Fig. 3, E and F) affords the net carrier density. The net electron (red) and hole (blue) densities at t = +20 ps (from Eqs. 1 and 2) in Fig. 3, A and D, are shown as dotted curves. Taking p-type as an example, electrons with initial velocity toward the junction are transported to n-type, whereas holes moving toward the junction face an impassable barrier. This gating behavior is illustrated in Fig. 3A (charges initially from p-type) and Fig. 3D (charges initially from n-type). The net charge separation leads to localization of electrons on one side and holes on the other, shown as shaded regions. This creates a long-range electric field, the potential of which is given in Fig. 4.

The sum of these four images, weighted to reflect the increased absorption in p-type, is presented in Fig. 4A. The figure depicts the long-range separation of carriers in agreement with the experimental observations. Separation due to the gating effect creates a net carrier distribution localized across the junction. The resultant Coulomb interactions distort the electric potential landscape as illustrated in Fig. 4B. For comparison, we present an experimental contrast image (Fig. 4C), which mirrors the net carrier distribution, and a potential map (Fig. 4D) calculated directly from the experimental data. Comparison between simulation and experiment shows agreement on the spatial extent of the distortions; this agreement validates the ballistic expansion of carriers as the underlying mechanism. The resulting electric potential, which opposes the intrinsic built-in junction potential, acts as spatiotemporally isolated "forward bias." At high fluences, this distortion induces a larger restoring force, which explains the fluence-dependent recombination rates observed in fig. S11.

Four-dimensional space-time imaging of carrier dynamics at interfaces, using SUEM, has the potential of unraveling in other complex structures the mechanism of charge transport, with ultrafast time resolution and nanometer-scale scanning capability. The unexpected ballistic carrier velocity (toward the junction) and the gated localization of charges (at the junction) are not predicted by the widely accepted drift-diffusion model, and these features may be characteristics of other materials when examined with the spatiotemporal resolutions of SUEM. At interfaces, the created transient density and electric field are dependent on the optical excitation, and it should be possible to control the properties of nano-to-micrometer–scale heterojunctions using the temporal, spatial, and pulse-shape characteristics of applied light fields.

REFERENCES AND NOTES

1. K.-T. Tsen, Ed., *Ultrafast Dynamical Processes in Semiconductors* (Springer-Verlag, New York, 2004).
2. J. Shah, *Ultrafast Spectroscopy of Semiconductors and Semiconductor Nanostructures* (Springer-Verlag, New York, 1999).
3. D. H. Auston, *Top. Appl. Phys.* **60**, 183–233 (1993).
4. P. Rodgers, Ed., *Nanoscience and Technology: A Collection of Reviews from Nature Journals* (World Scientific, London, 2010).
5. M. Saraniti, U. Ravaioli, *Nonequilibrium Carrier Dynamics in Semiconductors: Proceedings of the 14th Iinternational Conference, July 25-29, 2005, Chicago, USA* (Springer Proceedings in Physics, Berlin, 2006).
6. P. Hommelhoff, M. F. Kling, M. I. Stockman, *Ann. Phys.* **525**, A13–A14 (2013).
7. R. P. Prasankumar, P. C. Upadhya, A. J. Taylor, *Phys. Status Solidi B.* **246**, 1973–1995 (2009).
8. A. H. Zewail, *Science* **328**, 187–193 (2010).
9. R. Brunetti *et al*., *J. Appl. Phys.* **52**, 6713–6722 (1981).
10. O. F. Mohammed, D. S. Yang, S. K. Pal, A. H. Zewail, *J. Am. Chem. Soc.* **133**, 7708–7711 (2011).
11. Y. Lin, D. C. Joy, *Surf. Interface Anal.* **37**, 895–900 (2005).
12. S. Schäfer, W. X. Liang, A. H. Zewail, *Chem. Phys. Lett.* **493**, 11–18 (2010).
13. J. Goldstein *et al*., *Scanning Electron Microscopy and X-ray Microanalysis* (Springer, New York, 2007).
14. B. Sapoval, C. Hermann, *Physics of Semiconductors* (Springer-Verlag, New York, 1995).
15. K. W. A. Chee, C. Rodenburg, C. J. Humphreys, *J. Phys. Conf. Ser.* **126**, 012033 (2008).
16. K. W. A. Chee, C. Rodenburg, C. J. Humphreys, *Microscopy of Semiconducting Materials 2007*, A. G. Cullis, P. A. Midgley, Eds. (Springer-Verlag, Berlin, 2008).
17. S. L. Elliott, R. F. Broom, C. J. Humphreys, *J. Appl. Phys.* **91**, 9116–9122 (2002).
18. C. P. Sealy, M. R. Castell, P. R. Wilshaw, *J. Electron Microsc.* **49**, 311–321 (2000).
19. G. E. Jellison Jr., F. A. Modine, C. W. White, R. F. Wood, R. T. Young, *Phys. Rev. Lett.* **46**, 1414–1417 (1981).

ACKNOWLEDGMENTS

This work was supported by NSF grant DMR-0964886 and Air Force Office of Scientific Research grant FA9550-11-1-0055 in the Physical Biology Center for Ultrafast Science and Technology at California Institute of Technology, which is supported by the Gordon and Betty Moore Foundation.

SUPPLEMENTARY MATERIALS

www.sciencemag.org/content/347/6218/164/suppl/DC1
Materials and Methods
Supplementary Text
Figs. S1 to S11
Movies S1 to S3
References (*20*–*24*)

8 October 2014; accepted 2 December 2014
10.1126/science.aaa0217

QUANTUM GASES

Critical dynamics of spontaneous symmetry breaking in a homogeneous Bose gas

Nir Navon,*† Alexander L. Gaunt,† Robert P. Smith, Zoran Hadzibabic

Kibble-Zurek theory models the dynamics of spontaneous symmetry breaking, which plays an important role in a wide variety of physical contexts, ranging from cosmology to superconductors. We explored these dynamics in a homogeneous system by thermally quenching an atomic gas with short-range interactions through the Bose-Einstein phase transition. Using homodyne matter-wave interferometry to measure first-order correlation functions, we verified the central quantitative prediction of the Kibble-Zurek theory, namely the homogeneous-system power-law scaling of the coherence length with the quench rate. Moreover, we directly confirmed its underlying hypothesis, the freezing of the correlation length near the transition. Our measurements agree with a beyond-mean-field theory and support the expectation that the dynamical critical exponent for this universality class is z = 3/2.

Continuous symmetry-breaking phase transitions are ubiquitous, from the cooling of the early universe to the λ transition of superfluid helium. Near a second-order transition, critical long-range fluctuations have a diverging correlation length ξ, and details of the short-range physics are largely unimportant. Consequently, all systems can be classified into a small number of universality classes, according to their generic features such as symmetries, dimensionality, and range of interactions (*1*). Close to the critical point, many physical quantities exhibit power-law behaviors governed by critical exponents characteristic of a universality class. Specifically, for a classical phase transition, $\xi \sim |(T-T_c)/T_c|^{-\nu}$, where T_c is the critical temperature and ν is the (static) correlation-length critical exponent. Importantly, the corresponding relaxation time τ, needed to establish a diverging ξ, also diverges: $\tau \sim \xi^z$, where z is the dynamical critical exponent (*2*). An elegant framework for understanding the implications of this critical slowing down for the dynamics of symmetry breaking is provided by the Kibble-Zurek (KZ) theory (*3*, *4*).

Qualitatively, as T is reduced toward T_c at a finite rate, beyond some point in time the correlation length can no longer adiabatically follow its diverging equilibrium value. Consequently, at time $t = t_c$, the transition occurs without ξ ever having reached the size of the whole system. This results in the formation of finite-sized domains that display independent choices of the symmetry-breaking order parameter (Fig. 1A). [At the domain

Cavendish Laboratory, University of Cambridge, J. J. Thomson Avenue, Cambridge CB3 0HE, UK.
***Corresponding author. E-mail: nn270@cam.ac.uk** †These authors contributed equally to this work.

boundaries, rare long-lived topological defects can also form (*5*), their nature and density depending on the specific physical system.] Such domain formation was discussed in a cosmological context and linked to relativistic causality (*3*), whereas the connection to laboratory systems, critical slowing down, and universality classes was made in (*4*).

The main quantitative prediction of the KZ theory is that, under some generic assumptions (*5*), the average domain size d follows a universal scaling law. The crucial KZ hypothesis is that in the nonadiabatic regime close to t_c, the correlations remain essentially frozen. Then, for a smooth temperature quench, the theory predicts

$$d = \lambda_0 \left(\frac{\tau_Q}{\tau_0}\right)^b \quad (1)$$

with the KZ exponent

$$b = \frac{\nu}{1+\nu z} \quad (2)$$

where τ_Q is the quench time defined so that close to the transition $T/T_c = 1 + (t_c - t)/\tau_Q$, and λ_0 and τ_0 are a system-specific microscopic length scale and time scale, respectively.

Signatures of KZ physics have been observed in a wide range of systems, including liquid crystals (*6*), liquid helium (*7*, *8*), superconductors (*9*–*11*), atomic Bose-Einstein condensates (BECs) (*12*–*18*), multiferroics (*19*), and trapped ions (*20*–*22*). However, despite this intense activity, a direct quantitative comparison with Eqs. 1 and 2 has remained elusive; some common complications include system inhomogeneity, modified statistics of low-probability defects, and uncertainties over the nature of the transition being crossed [for a recent review, see (*5*)]. In this work, we studied the dynamics of spontaneous symmetry breaking in a homogeneous atomic Bose gas, which is in the same universality class as the three-dimensional (3D) superfluid ^{4}He. For this class, mean-field (MF) theory predicts $\nu = 1/2$ and $z = 2$, giving $b = 1/4$, whereas a beyond-MF dynamical critical theory, the so-called F model (*2*), gives $\nu \approx 2/3$ and $z = 3/2$, so $b \approx 1/3$. We prepared a homogeneous Bose gas by loading 3×10^5 ^{87}Rb atoms into a cylindrical optical-box trap (*23*) of length $L \approx 26$ μm along the horizontal x axis and radius $R \approx 17$ μm. Initially, $T \approx 170$ nK, corresponding to $T/T_c \approx 2$. We then evaporatively cooled the gas by lowering the trap depth, crossed $T_c \approx 70$ nK with 2×10^5 atoms, and had 10^5 atoms at $T \lesssim 10$ nK ($T/T_c \lesssim 0.2$). In our system, λ_0 is expected to be set by the thermal wavelength at the critical point, $\lambda_c \approx 0.7$ μm, and τ_0 by the elastic scattering time τ_{el} (*13*, *24*); for our parameters, a classical estimate gives $\tau_{el} \approx 30$ ms.

Qualitatively, random phase inhomogeneities in rapidly quenched clouds are revealed in time-of-flight (TOF) expansion as density inhomogeneities (*14*, *25*), such as shown in Fig. 1B (here the gas was cooled to $T << T_c$ in 1 s). In our finite-sized box, we can also produce essentially pure and fully coherent (single-domain) BECs, by cooling the gas slowly (over ≳5 s). In TOF, such a BEC develops the characteristic diamond shape (*26*) seen in Fig. 1C.

To quantitatively study the coherence of our clouds, we probed the first-order two-point correlation function

$$g_1(\boldsymbol{r}, \boldsymbol{r}') \propto \langle \hat{\Psi}^\dagger(\boldsymbol{r})\, \hat{\Psi}(\boldsymbol{r}') \rangle \quad (3)$$

where $\hat{\Psi}(\boldsymbol{r})$ is the Bose field. Our method (Fig. 2A) is inspired by (*27*). We use a short (0.1 ms) Bragg-diffraction light pulse to create a small copy of the cloud (containing ≈5% of the atoms) moving along the x axis with recoil velocity $v_r \approx 3$ mm/s (*26*). A second identical pulse is applied a time Δt later, when the two copies are shifted by $x = v_r \Delta t$ and for $x < L$ still partially overlap. This results in interference of the two displaced copies of the cloud in the overlap region of length $L - x$. After the second Bragg pulse, the fraction of diffracted atoms (for $x < L$) is (*28*)

$$\frac{N_r}{N} = \frac{1}{2}\left[1 + \left(1 - \frac{x}{L}\right) g_1(x)\right] \sin^2\theta \quad (4)$$

where $g_1(x) \equiv \mathrm{Re}[g_1(\boldsymbol{r}, \boldsymbol{r} + x\hat{\boldsymbol{x}})]$ is the correlation function corresponding to periodic boundary conditions and normalized so that $g_1(0) = 1$, and θ is the area of each Bragg pulse (in our case $\theta \approx \pi/7$). Allowing the recoiling atoms to fully separate from the main cloud (in 140 ms of TOF) and counting N_r and N, we directly measured $G_1(x) \equiv (1 - x/L) g_1(x)$, with a spatial resolution of ≈0.7 μm. Our resolution was limited by the duration of the Bragg pulses and the (inverse) recoil momentum; we experimentally assessed it by measuring G_1 in a thermal cloud with a thermal wavelength <0.5 μm.

In Fig. 2B we show examples of $G_1(x)$ functions measured in equilibrium (blue) and after a quench (red). In an essentially pure equilibrium BEC (prepared slowly, as for Fig. 1C), $g_1(x) = 1$ and $G_1(x)$ is simply given by the triangular function $1 - x/L$ (dark blue solid line). In equilibrium at $T/T_c \approx 0.7$, we see a fast initial decay of G_1, reflecting the significant thermal fraction. However, importantly, the coherence still spans the whole system, with the slope of the long-ranged part of G_1 giving the condensed fraction (light blue line is a guide to the eye). By comparison, the G_1 functions for quenched clouds clearly have no equilibrium interpretation. Here $T/T_c \approx 0.2$, corresponding to a phase space density >25, and yet coherence extends over only a small fraction of L. These data are fitted well by $g_1 \propto \exp(-x/\ell)$ (red lines), which provides a simple and robust way to extract the coherence length. This exponential form is further supported by a 1D calculation shown in the inset of Fig. 2B. Here we generated a wave function with a fixed number of domains $\mathcal{D}$, randomly positioning the domain walls and assigning each domain a random phase. Averaging over many realizations, we obtained $g_1(x)$ that is fitted very well by an exponential with $\ell = L/\mathcal{D} = d$. (In our 3D experiments, the total number of domains was $\sim\mathcal{D}^3$ and $g_1(x)$ was effectively averaged over $\sim\mathcal{D}^2$ 1D distributions.)

We now turn to a quantitative study of ℓ for different quench protocols (Fig. 3). For the KZ scaling law of Eqs. 1 and 2 to hold, a crucial assumption is that the correlation length is essentially frozen in time near t_c. Specifically, for $\nu z = 1$, which in our case holds for both MF theory and the F model, the freeze-out time of ℓ for $t > t_c$ is expected to be (*4*)

$$\hat{t} = f\sqrt{\tau_Q \tau_0}, \quad (5)$$

where f is a dimensionless number of order unity. Although intuitively appealing, this assumption is in principle only approximative, and the dynamics

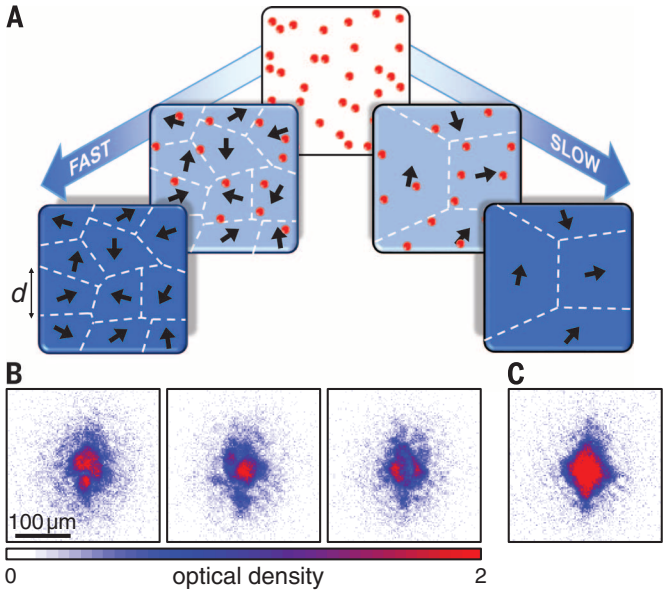

Fig. 1. Domain formation during spontaneous symmetry breaking in a homogeneous Bose gas. (**A**) Red points depict thermal atoms and blue areas coherent domains, in which the $U(1)$ gauge symmetry is spontaneously broken. The arrows indicate the independently chosen condensate phase at different points in space, and dashed lines delineate domains over which the phase is approximately constant. The average size d of the domains formed at the critical point depends on the cooling rate. Further cooling can increase the population of each domain before the domain boundaries evolve. (**B**) Phase inhomogeneities in a deeply degenerate gas are revealed in TOF expansion as density inhomogeneities. Shown are three realizations of cooling the gas in 1 s from $T \approx 170$ nK, through $T_c \approx 70$ nK, to ≲10 nK. Each realization of the experiment results in a different pattern, and averaging over many images results in a smooth, featureless distribution. (**C**) Preparing a $T \lesssim 10$ nK gas more slowly (over 5 s) results in an essentially pure BEC with a spatially uniform phase.

of the system coarsening (i.e., merging of the domains) at times $t > t_c$ is still a subject of theoretical work (*29*). Practically, a crucial question is when one should measure ℓ in order to verify the universal KZ scaling. We resolved these issues by using two different quench protocols outlined in Fig. 3A, which allow us both to observe the KZ scaling and to directly verify the freeze-out hypothesis, without an a priori knowledge of the exact values of f and τ_0.

In the first quench protocol (QP1), we followed cooling trajectories such as shown in Fig. 3A and varied only the total cooling time t_Q. We restricted t_Q to values between 0.2 and 3.5 s, for which we observed that the cooling curves were self-similar (as seen in Fig. 3A). We always crossed $T_c = 70(10)$ nK at $t_c = 0.72(5)t_Q$ (vertical dashed line) and always had the same atom number (within ±20%) at the end of cooling. The self-similarity of the measured cooling trajectories and the essentially constant evaporation efficiency indicate that for this range of t_Q values, the system is always sufficiently thermalized, the temperature (as determined from the thermal wings in TOF) is well defined during the quench (*30*), and to a good approximation τ_Q is simply proportional to t_Q. (For $t_Q < 0.2$ s, the evaporation is less efficient and the cooling trajectories are no longer self-similar.)

In Fig. 3B we plot ℓ versus t_Q, measured using QP1 (blue points). For $t_Q \leq 1$ s, we observed a slow power-law growth of ℓ, in good agreement with the expected KZ scaling (blue shaded area). However, for longer t_Q, this scaling breaks down and ℓ grows faster, quickly approaching the system size. Importantly, this breakdown can also be fully understood within the KZ framework. We note that the time between crossing T_c and the end of cooling is $t_Q - t_c \approx 0.28\ t_Q \propto t_Q$, whereas the KZ freeze-out time is $\hat{t} \propto \sqrt{\tau_Q} \propto \sqrt{t_Q}$, so for slow enough quenches, $t_Q - t_c$ inevitably exceeds $\hat{t}$. Hence, although it may be impossible to adiabatically cross T_c, in practice the system can unfreeze and heal significantly before it is observed (*31*). From the point where the KZ scaling breaks down in Fig. 3B, $t_Q^{br} \approx 1$ s, we posit that for $t_Q = t_Q^{br}$, we have $\hat{t} \approx 0.28\ t_Q^{br}$ and hence, from Eq. 5, more generally $\hat{t} \approx 0.28\sqrt{t_Q t_Q^{br}}$.

To verify this picture, we employed a second quench protocol (QP2), which involved two cooling steps, as shown by the orange points in the bottom panel of Fig. 3A. We initially followed the QP1 trajectory for a given t_Q, but then at a variable "kink" time $t_k \gtrsim t_c$, we accelerated the cooling; the last part of the trajectory always corresponds to the final portion of our fastest, 0.2-s cooling trajectory. This way, even for $t_Q > t_Q^{br}$ we can complete the cooling and measure g_1 before the system has time to unfreeze.

In Fig. 3C, the orange points show the QP2 measurements of ℓ for $t_Q = 3.2$ s and various values of the kink position t_k/t_Q. These data reveal two notable facts. First, for a broad range of t_k values, ℓ is indeed constant (within errors), and the width of this plateau agrees with our estimate $\hat{t} \approx 0.5$ s for $t_Q = 3.2$ s, indicated by the horizontal arrow. Second, the value of ℓ within the plateau region falls in line with the KZ scaling law in Fig. 3B. We also show analogous QP2

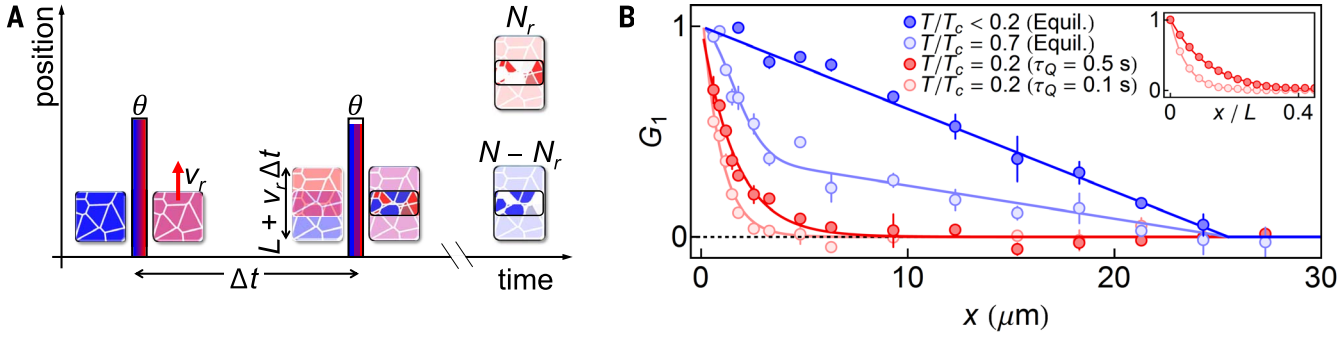

Fig. 2. Two-point correlation functions in equilibrium and quenched gases. (**A**) Homodyne interferometric scheme. The first Bragg-diffraction pulse (θ) creates a superposition of a stationary cloud and its copy moving with a center-of-mass velocity v_r. After a time Δt, a second pulse is applied. In the region where the two copies of the cloud displaced by $x = v_r\Delta t$ overlap, the final density of the diffracted atoms depends on the relative phase of the overlapping domains; $g_1(x)$ is deduced from the diffracted fraction N_r/N (see text). (**B**) Correlation function $G_1(x) = (1 - x/L)g_1(x)$ measured in equilibrium (blue) and after a quench (red) for, respectively, two different T/T_c values and two different quench times. (Inset) 1D calculation of G_1 for a fragmented BEC containing $\mathcal{D} = 10$ (red) and 20 (light red) domains of random sizes and phases. The solid lines correspond to $g_1 = \exp(-x\mathcal{D}/L)$.

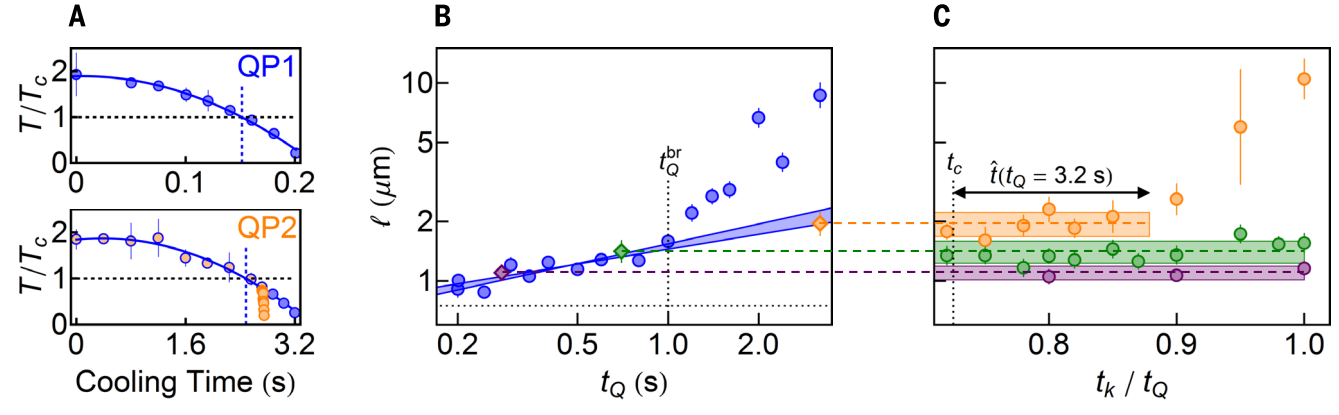

Fig. 3. KZ scaling and freeze-out hypothesis. (**A**) Quench protocols. The self-similar QP1 trajectories are shown in blue for total cooling time $t_Q = 0.2$ s (upper panel) and 3.2 s (lower panel). We use polynomial fits to the data (solid lines) to deduce t_c and τ_Q. QP2 is shown in the lower panel by the orange points, with the kink at $t_k = 0.85\ t_Q$. (**B**) Coherence length ℓ as a function of t_Q. Blue points correspond to QP1. The shaded blue area shows power-law fits with $1/4 < b < 1/3$ to the data with $t_Q \leq t_Q^{br} = 1$ s. The horizontal dotted line indicates our instrumental resolution. (**C**) Coherence length ℓ measured following QP2, as a function of t_k/t_Q, for $t_Q = 3.2$ s (orange), 0.7 s (green), and 0.3 s (purple). The shaded areas correspond to the essentially constant ℓ (and its uncertainty) in the freeze-out period $t_k - t_c < \hat{t}$. (For $t_Q < t_Q^{br}$ the system never unfreezes.) The (average) ℓ values within these plateaus are shown in their respective colors as diamonds in (B).

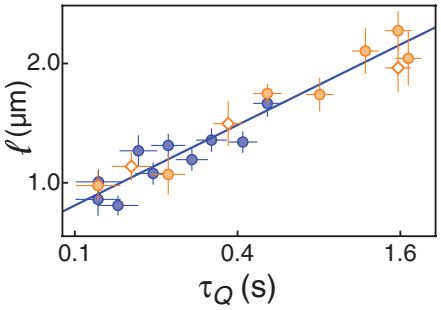

Fig. 4. Critical exponents of the interacting BEC transition. Orange circles and diamonds show ℓ values obtained using QP2, as in Fig. 3C; the diamonds show the same three data points as in Fig. 3B. Blue circles show the same QP1 data, with $t_Q \leq 1$ s as in Fig. 3B. We obtained $b = 0.35(4)$ (solid line), in agreement with the F-model prediction $b \approx 1/3$, corresponding to $\nu \approx 2/3$ and $z = 3/2$, and excluding the mean-field value $b = 1/4$.

measurements for $t_Q = 0.7$ s (green) and 0.3 s (purple); in these cases, $t_Q < t_Q^{br}$, so $\hat{t}$ is longer than $t_Q - t_c$, the system never unfreezes, and thus the acceleration of the cooling has no effect on ℓ. These results provide direct support for the KZ freeze-out hypothesis.

To accurately determine the KZ exponent b, we made extensive measurements following QP2, extracting ℓ from the plateaued regions of width $\min[\hat{t}, t_Q - t_c]$, as in Fig. 3C. In Fig. 4, we combine these data with the QP1 measurements for $t_Q \leq 1$ s, and plot ℓ versus τ_Q. The plotted values of τ_Q and their uncertainties include the small systematic variation of the derivative of our cooling trajectory between t_c and $t_c - \hat{t}$. We finally obtain $b = 0.35(4)$, which strongly favors the F-model prediction $b \approx 1/3$ over the MF value $b = 1/4$ (*32*).

Having observed excellent agreement with the KZ theory, we discuss the implications of our measurements for the critical exponents of the interacting BEC phase transition, which is in the same universality class as the λ transition of ^{4}He. Whereas $\nu \approx 0.67$ has been measured in both liquid helium [see (*33*)] and atomic gases (*34*), the dynamical exponent z has presented a challenge to experiments [see (*2*, *35*)]. Using the well-established $\nu = 0.67$ and Eq. 2, we obtain $z = 1.4(4)$. In contrast, MF theory does not provide a self-consistent interpretation of our results, as fixing $\nu = 1/2$ yields an inconsistent $z = 0.9(4)$. Interestingly, if we instead fix $\nu z = 1$, which holds at both the MF and F-model levels, from Eq. 2 we obtain a slightly more precise $z = 1.4(2)$ and also recover $\nu = 0.70(8)$.

It would be interesting to study the effect of tunable interactions in a homogeneous atomic gas on the value of b. According to the Ginzburg criterion, near the critical point, MF breaks down for $\xi \gtrsim \xi_G = \lambda_c^2/(\sqrt{128}\pi^2 a)$, where a is the s-wave scattering length. It is tempting to combine the (dynamical) KZ and (equilibrium) Ginzburg arguments and speculate that one should observe the MF value of b if on approach to T_c the KZ freeze-out occurs before MF breaks down, and the F value of b if the reverse is true. In our experiments, $\xi_G \approx 0.8$ μm and the freeze-out values of ℓ are systematically higher. However, with use of a Feshbach resonance, the opposite regime should be within reach. Another interesting study could focus on the dynamics of domain coarsening. Finally, our methods could potentially be extended to studies of higher-order correlation functions and the full statistics of the domain sizes.

REFERENCES AND NOTES

1. M. Kardar, *Statistical Physics of Fields* (Cambridge Univ. Press, Cambridge, 2007).
2. P. C. Hohenberg, B. I. Halperin, *Rev. Mod. Phys.* **49**, 435–479 (1977).
3. T. W. B. Kibble, *J. Phys. A* **9**, 1387–1398 (1976).
4. W. H. Zurek, *Nature* **317**, 505–508 (1985).
5. A. del Campo, W. H. Zurek, *Int. J. Mod. Phys. A* **29**, 1430018 (2014).
6. I. Chuang, R. Durrer, N. Turok, B. Yurke, *Science* **251**, 1336–1342 (1991).
7. C. Bäuerle, Y. M. Bunkov, S. Fisher, H. Godfrin, G. Pickett, *Nature* **382**, 332–334 (1996).
8. V. Ruutu *et al.*, *Nature* **382**, 334–336 (1996).
9. R. Carmi, E. Polturak, *Phys. Rev. B* **60**, 7595–7600 (1999).
10. R. Carmi, E. Polturak, G. Koren, *Phys. Rev. Lett.* **84**, 4966–4969 (2000).
11. R. Monaco, J. Mygind, R. J. Rivers, *Phys. Rev. Lett.* **89**, 080603 (2002).
12. L. E. Sadler, J. M. Higbie, S. R. Leslie, M. Vengalattore, D. M. Stamper-Kurn, *Nature* **443**, 312–315 (2006).
13. C. N. Weiler *et al.*, *Nature* **455**, 948–951 (2008).
14. D. Chen, M. White, C. Borries, B. DeMarco, *Phys. Rev. Lett.* **106**, 235304 (2011).
15. G. Lamporesi, S. Donadello, S. Serafini, F. Dalfovo, G. Ferrari, *Nat. Phys.* **9**, 656–660 (2013).
16. S. Braun *et al.*, http://arxiv.org/abs/1403.7199 (2014).
17. L. Corman *et al.*, *Phys. Rev. Lett.* **113**, 135302 (2014).
18. L. Chomaz *et al.*, http://arxiv.org/abs/1411.3577 (2014).
19. S. C. Chae *et al.*, *Phys. Rev. Lett.* **108**, 167603 (2012).
20. S. Ulm *et al.*, *Nat. Commun.* **4**, 2290 (2013).
21. K. Pyka *et al.*, *Nat. Commun.* **4**, 2291 (2013).
22. S. Ejtemaee, P. Haljan, *Phys. Rev. A* **87**, 051401(R) (2013).
23. A. L. Gaunt, T. F. Schmidutz, I. Gotlibovych, R. P. Smith, Z. Hadzibabic, *Phys. Rev. Lett.* **110**, 200406 (2013).
24. J. R. Anglin, W. H. Zurek, *Phys. Rev. Lett.* **83**, 1707–1710 (1999).
25. S. Dettmer *et al.*, *Phys. Rev. Lett.* **87**, 160406 (2001).
26. I. Gotlibovych *et al.*, *Phys. Rev. A* **89**, 061604(R) (2014).
27. E. W. Hagley *et al.*, *Phys. Rev. Lett.* **83**, 3112–3115 (1999).
28. See the supplementary materials on *Science* Online.
29. G. Biroli, L. F. Cugliandolo, A. Sicilia, *Phys. Rev. E* **81**, 050101(R) (2010).
30. Near T_c, the mean free path for classical elastic collisions is about four times larger than the size of the box. Hence, although the evaporation takes place at the box walls, we can also safely assume that T is uniform across the sample.
31. The unfreezing and healing of the system reconcile the small $b \approx 0.3$ and the fact that a fully coherent homogeneous BEC (as in Fig. 1C) can be produced in a relatively modest cooling time, $\sim 10^2 \tau_{el}$. In harmonically trapped Bose gases, $b \geq 1$ is observed (*5*, *15*), which makes the physics significantly different. In that case, cooling with $\tau_Q \sim 10^2 \tau_{el}$ is sufficiently slow to directly produce essentially fully coherent BECs.
32. Scaling ℓ to λ_c and τ_Q to τ_{el}, for each data series separately, affects b by <0.01.
33. A. A. Pogorelov, I. M. Suslov, *JETP Lett.* **86**, 39–45 (2007).
34. T. Donner *et al.*, *Science* **315**, 1556–1558 (2007).
35. R. Folk, G. Moser, *J. Phys. A* **39**, R207–R313 (2006).

ACKNOWLEDGMENTS

We thank M. Robert-de-Saint-Vincent for experimental assistance; R. Fletcher for comments on the manuscript; and N. Cooper, J. Dalibard, G. Ferrari, B. Phillips, and W. Zwerger for insightful discussions. This work was supported by AFOSR, ARO, DARPA OLE, and EPSRC (grant no. EP/K003615/1). N.N. acknowledges support from Trinity College, Cambridge, and R.P.S. from the Royal Society.

SUPPLEMENTARY MATERIALS

www.sciencemag.org/content/347/6218/167/suppl/DC1
Methods
Fig. S1

14 July 2014; accepted 5 December 2014
10.1126/science.1258676

GUT MICROBIOTA

Antimicrobial peptide resistance mediates resilience of prominent gut commensals during inflammation

T. W. Cullen,[1,2] W. B. Schofield,[1,2] N. A. Barry,[1,2] E. E. Putnam,[1,2] E. A. Rundell,[1] M. S. Trent,[3] P. H. Degnan,[4] C. J. Booth,[5] H. Yu,[6] A. L. Goodman[1,2]*

Resilience to host inflammation and other perturbations is a fundamental property of gut microbial communities, yet the underlying mechanisms are not well understood. We have found that human gut microbes from all dominant phyla are resistant to high levels of inflammation-associated antimicrobial peptides (AMPs) and have identified a mechanism for lipopolysaccharide (LPS) modification in the phylum Bacteroidetes that increases AMP resistance by four orders of magnitude. *Bacteroides thetaiotaomicron* mutants that fail to remove a single phosphate group from their LPS were displaced from the microbiota during inflammation triggered by pathogen infection. These findings establish a mechanism that determines the stability of prominent members of a healthy microbiota during perturbation.

Human gut microbial communities reside in an open ecosystem subject to disruptions ranging from dietary change to toxin exposure and pathogen invasion. Many of these perturbations, and functional disorders such as irritable bowel syndrome, are accompanied by nonspecific immune responses that disrupt community structure and function (*1*, *2*). Host inflammatory mechanisms to remove harmful organisms and restrict bacteria to the lumen

Science

Critical dynamics of spontaneous symmetry breaking in a homogeneous Bose gas

Nir Navon, Alexander L. Gaunt, Robert P. Smith, and Zoran Hadzibabic

Science, 347 (6218),

Breaking the symmetry in an atomic gas

Cooling a physical system through a phase transition typically makes it less symmetrical. If the cooling is done very slowly, this symmetry change is uniform throughout the system. For a faster cooling process, the system breaks up into domains: The faster the cooling, the smaller the domains. Navon *et al.* studied this process in an ultracold gas of Rb atoms near its transition to a condensed state (see the Perspective by Ferrari). The authors found that the size of the domains froze in time in the vicinity of the transition and that it depended on the cooling speed, as predicted by theory.

Science, this issue p. 167; see also p. 127

Science (ISSN 1095-9203) is published by the American Association for the Advancement of Science. 1200 New York Avenue NW, Washington, DC 20005. The title *Science* is a registered trademark of AAAS.